FANCD2 counteracts O^6-methylguanine-induced mismatch repair-dependent apoptosis

Sho Morita[1,2], Ryosuke Fujikane[1,3*], Yuka Uechi[1], Takashi Matsuura[2], and Masumi Hidaka[1,3]

[1] Department of Physiological Science and Molecular Biology, Fukuoka Dental College, 2-15-1, Tamura, Sawaraku, 814-0193, Fukuoka, Japan
[2] Department of Oral Rehabilitation, Fukuoka Dental College, 2-15-1, Tamura, Sawaraku, 814-0193, Fukuoka, Japan
[3] Oral Medicine Research Center, Fukuoka Dental College, 2-15-1, Tamura, Sawaraku, 814-0193, Fukuoka, Japan
*Corresponding author. E-mail: fujikane@fdcnet.ac.jp

ORCID
Ryosuke Fujikane: 0000-0002-6621-3848
Masumi Hidaka: 0000-0002-1901-2955

Abstract

Background

Sn1-type alkylating agents methylate the oxygen atom on guanine bases thereby producing O^6-methylguanine. This modified base could pair with thymine and cytosine, resulting in the formation of O^6-methylguanine/thymine mismatch during DNA replication, recognized by the mismatch repair (MMR) complex, which then initiates the DNA damage response and subsequent apoptotic processes. In our investigation of the molecular mechanisms underlying MMR-dependent apoptosis, we observed FANCD2 modification upon the activity of alkylating agent N-methyl-N-nitrosourea (MNU). This observation led us to hypothesize a relevant role for FANCD2 in the apoptosis induction process.

Methods and Results

We generated FANCD2 knockout cells using the CRISPR/Cas9 method in the human cervical cancer cell line HeLa MR. FANCD2-deficient cells exhibited MNU hypersensitivity. Upon MNU exposure, FANCD2 colocalized with the MMR complex. MNU-treated FANCD2 knockout cells displayed severe S phase delay followed by increased G2/M arrest and MMR-dependent apoptotic cell death. Moreover, FANCD2 knockout cells exhibited impaired CtIP and RAD51 recruitment to the damaged chromatin and DNA double-strand break accumulation, indicated by simultaneously observed increased γH2AX signal and 53BP1 foci.

Conclusions

Our data suggest that FANCD2 is crucial for recruiting homologous recombination factors to the sites

of the MMR-dependent replication stress to resolve the arrested replication fork and counteract O^6-methylguanine-triggered MMR-dependent apoptosis.

Keywords: Mismatch repair, Fanconi anemia, DNA damage response, Apoptosis, Alkylating agent

Introduction

The mismatch repair (MMR) system removes nucleotides misincorporated into the nascent strand during DNA replication and contributes to replication fidelity improvement and genome homeostasis. The mismatch recognition complex, MutSα (MSH2/MSH6 heterodimer) and MutLα (MLH1/PMS2 heterodimer) performs the MMR reaction, followed by exonuclease activity, such as that of EXO1, MRE11, and ARTEMIS as well as replication factors PCNA, RPA, RFC, DNA polymerase, and DNA ligase [1-3]. Beyond the canonical mismatch repair, the MMR system also contributes to maintaining genome homeostasis by eliminating cancer-prone cells carrying the mutagenic and cytotoxic base, O^6-methylguanine (O^6-meG), produced on the DNA by Sn1-type methylating agents, such as N-methyl-N-nitrosourea (MNU) and N-methyl-N-nitro-N-nitrosoguanidine (MNNG) [4-6]. Although O^6-meG is repaired by O^6-methylguanine DNA-methyltransferase (MGMT), which transfers the methyl group from the guanine onto a cysteine residue in its active site [7,8], persistent O^6-meGs could form mispairs with thymines at a rate similar to that of cytosine during DNA replication, resulting in G:C-to-A:T transition mutation following the upcoming DNA replication phase. To prevent such outcomes, the MMR complex recognizes the O^6-meG/T mismatch and induces apoptosis to eliminate the affected cells [4,9]. During the apoptosis induction process, DNA damage responses are activated and occur through phosphorylation by protein kinases, ATR/CHK1 and ATM/CHK2, which respond to replication stress and DNA double-strand break (DSB), respectively [10,11]. Next cell cycle progression gets arrested MMR-dependently at the G2/M phase of the second round of the cycle, followed by caspase activation, leading to apoptosis [10,12-15].

The MMR-dependent cytotoxic effect could be explained by two hypotheses: the futile repair cycle and the direct signaling models. In the former case, the MMR system recognizes the O^6-meG/T mismatch and attempts its reparation. However, thymine is repeatedly incorporated into the site opposite to O^6-meG on the template strand during the repair reaction. The futile MMR reactions leave ssDNA gaps around the O^6-meG/T mismatch, converted into DSBs during the upcoming DNA replication round, and activate apoptosis induction [15,16]. In the latter model, the MMR complex directly activates the ATR to initiate DNA damage responses, followed by apoptosis induction. This concept is supported by an *in vitro* reconstitution assay yielding O^6-meG/T-bound MMR complex interaction with ATR, phosphorylating CHK1 [17-19]. The former model explains G2/M arrest occurrence at the second cell cycle round after MNU treatment while the latter model cannot explain this step. Although genetic screening and proteomics analysis of proteins physically interacting with

MMR proteins have identified several MMR-dependent apoptotic pathway-involved proteins and genes, how cells regulate DNA damage-related processes during MMR-dependent apoptosis remains elusive.

We previously described that FANCD2- and FANCI-associated nuclease I (FAN1) interacts with MLH1 and is involved in apoptosis induction by producing single-stranded DNA (ssDNA) via exonuclease activity [20]. The aforementioned and previous studies have shown that FANCD2 forms nuclear foci upon MNU and temozolomide treatment [20,21]. FANCD2 is a Fanconi anemia-responsible gene involved in repairing Mitomycin C (MMC)-produced interstrand crosslinks (ICLs) and aphidicolin and hydroxyurea treatment-induced stalled replication forks [22,23]. When the replication fork encounters such problems, the Fanconi core complex associates with it and monoubiqutinates FANCD2 at the stalled replication fork [24,25]. The monoubiquitinated FANCD2 then serves as a scaffold for binding UBZ domain-containing proteins, such as FAN1 and SLX4, to resolve the complex structure of the stalled replication fork [23]. FANCD2 also protects the replication fork from the exonuclease-related excessive nascent DNA strand degradation, in order to avoid expanding the single-strand region, leading to DNA strand breaks [26,27]. While FANCD2 involvement in the stalled replication fork repair has been extensively investigated, FANCD2 function in the alkylating agent-induced MMR-dependent damage response remains poorly understood.

In this study, we discovered that FANCD2 is ubiquitinated and forms nuclear foci in an MMR-dependent manner, some of which colocalize with MLH1 upon MNU treatment. The FANCD2-knockout cells we constructed exhibited MNU hypersensitivity and increased 53BP1 foci number in the nucleus compared with the control. Our results suggest that the MMR complex formed on the O^6-meG/T mismatch induces replication stress, requiring FANCD2 activity to restart replication for survival.

Materials and Methods

Cell culture

The cell lines we used in this study as well as cell culture and treatment conditions with alkylating agents have been described previously [13,14]. Briefly, we obtained HeLa MR cells, a human MGMT-deficient cervical cancer cell line and MLH1-deficient cell line [28], from our laboratory stock and cultured in Dulbecco's Modified Eagle Medium (DMEM; Fujifilm Wako) supplemented with 10% FBS, streptomycin, and penicillin at 37°C in 5% CO_2. For the alkylating agent treatment, we incubated the cells with appropriate N-methyl-N-nitrosourea concentrations resolved in DMEM with 0.02-M HEPES-KOH (pH 6.0) for 1 h then further cultured in the medium until cell collection at the indicated time. For S phase synchronization, we cultured the cells in a media with 2.5-mM thymidine then without it for 16 and 8 h, respectively, followed by further culture with 2.5-mM thymidine for 16 h.

The synchronized cells were washed with the medium once, then released by culture in the medium.

Antibodies

The anti-phospho-S1981 ATM (#13050), -ATM (#2873), -Caspase9 (#9502), -phospho-S317 CHK1 (#12302), -CHK1 (#2360), -phosphor-T68 CHK2 (#2661), -CHK2 (#6334), -γH2AX (#7631), -CtIP (#9021), and anti-RPA32 (#35869) antibodies were purchased from Cell Signaling Tech. Anti-ß-actin (010-27841) was obtained from Fujifilm Wako. Anti-phospho-T1989 ATR (GTX128145) was purchased from Gene Tex. Anti-Lamin A/C antibody (sc7292), -FANCD2 (sc20022), and -ATR (sc1887) were obtained from Santa Cruz Biotech. Anti-MLH1 (554073) was purchased from BD Biosciences. Anti-FLAG M2 antibody (F1804) was purchased from Sigma. Anti-MSH2 antibody (337900) and the Alexa488- or Alexa568-conjugated anti-Mouse or -Rabbit antibodies were purchased from Thermo Fisher. Anti-RAD51 (#70-012) was purchased from BioAcademia and the anti-53BP1 antibody (MAB3802) from Merck-Millipore.

FANCD2 knockout cell line construction using CRISPR/Cas9

Guide RNAs were designed using the web-based program CRISPOR (http://crispor.tefor.net) [29] with the exon 3 sequence of the human FANCD2 gene as a query. We annealed the designed oligonucleotides, 5'-CACCGTAAAGCTTCTTAAGATATC-3' and 5'-aaacGATATCTTAAGAAGCTTTAC-3', ligated them into a BbsI-digested pX459 vector (Addgene# 62988) [30], and sequenced the construct. We transfected the resulting vector into HeLa MR cells and selected puromycin-resistant ones in the medium with 3 μg/mL puromycin for 2 days. We further cultured the cells in a medium without puromycin for 10 days and confirmed the FANCD2 gene knockout in the surviving clones by immunoblotting and Sanger sequencing of the target locus, which was cloned into the pMD20 vector (Takara Bio Inc.).

Gene knockdown

To knockdown specific genes, cells were transfected with MSH2-specific (#1; 5'-UAUAAUUCUUCCUUGUCCUUUCUCC-3') and (#2; 5'-GAGAAUGAUUGGUAUUUGGCAUAUA-3'); MLH1-specific (#1; 5'-UGCACAUUAACAUCCACAUUCUGGG-3') and (#2; 5'-GGAUGUUAAUGUGCACCCCACAAAG-3'); or CtIP-specific (#1; 5'-CAGCUGAGCUUGAAUGUGATT-3') and (#2; 5'-CAACACUUGUAUAUCUAGATT-3') siRNA using Lipofectamine RNAi MAX, following manufacturer's instructions (Thermo Fisher). Subsequently, the transfected cells were treated with MNU, and whole-cell extracts were prepared 2 or 3 days after transfection.

Survival assay

We treated 500 cells with MNU for 1 h, then cultured them in a medium without MNU for 10 days. We fixed the colonies formed with 10% formaldehyde for 10 min, followed by staining with 0.1% crystal violet. We counted the surviving colonies and calculated the survival ratios from three independent repeats.

Immunoblot analysis

We obtained whole-cell extracts by direct lysis of the cells with 2X Sodium dodecyl sulfate (SDS) sample buffer (100-mM Tris-HCl, pH6.8, 2% SDS, and 20% glycerol) and boiling for 10 min, followed by sonication if required. To prepare chromatin fractions, we treated the cells with mCSK buffer (10-mM PIPES-NaOH [pH 6.8], 100-mM NaCl, 300-mM sucrose, 1-mM EGTA, and 1-mM $MgCl_2$) containing 0.1% Triton X-100 for 10 min on ice and centrifuged for 10 min at 20,000 ×g. We lysed the precipitants by adding 2X SDS sample buffer and sonicating, then separated the soluble proteins using SDS-PAGE followed by electrotransferring onto a PVDF membrane (Bio-Rad) treated with the Can Get Signal blocking agent (Toyobo) for 2 h, followed by overnight incubation with 1:1,000 dilution an appropriate first antibody. Next, we treated the membrane with phosphate-buffered saline (PBS) containing 0.1% Tween 20 (PBST), then incubated it with HRP-conjugated anti-mouse or anti-rabbit IgG secondary antibodies. After extensive washing with PBST, we visualized the proteins by adding ImmunoStar LD reagent (Fujifilm Wako) and using LAS4000 (Cytiva), and quantified bands using 1D Image gauge software (Cytiva).

Immunoprecipitation

We treated the above-described HeLa MR cells with or without drugs (25-μM MNU or 10-μM Mitomycin C) for 1 h and cultured them in DMEM. Next, we treated the cells with a hypotonic buffer (20-mM HEPES-KOH [pH 7.5], 5-mM KCl, 1.5-mM $MgCl_2$, 0.1-mM DTT, and 100-μg/mL Digitonin) on ice for 10 min, washed with ice-cold PBS, and fixed with 1% formaldehyde at RT for 10 min. We quenched the formaldehyde by adding 50-mM Tris-HCl (pH 8.0), collected the cells with a scraper, then centrifuged them. We suspended the cells in RIPA buffer (50-mM Tris-HCl, [pH 8.0], 150-mM NaCl, 0.5% Deoxycholate, 1% NP40, and 0.1% SDS), then sonicated and centrifuged them for 10 min at 20,000 ×g. We supplemented the supernatant with 1 μg of anti-FANCD2 antibody and incubated the mix at 4°C for 1 h; followed by incubation with protein G agarose beads (Cytiva) overnight at 4°C. We then centrifuged the mixture and washed the precipitant extensively with RIPA buffer, lysed it with 2X SDS sample buffer, and subjected it to immunoblotting.

Immunofluorescence analysis

We treated the cells with or without 25-μM MNU for 1 h and cultured them in DMEM on a film

bottom dish (Matsunami Glass Ind.). We washed the cells with PBS, incubated them in mCSK buffer containing 0.1% Trition X-100 on ice for 10 min, and fixed them with 4% paraformaldehyde for 10 min at RT. We then washed the cells with PBS and incubated them with 2% bovine serum albumin in PBS for 2 h. We used 1/200-diluted anti-FANCD2, anti-MLH1, anti-Rad51, and anti-53BP1 primary antibodies and incubated the cells with Alexa488-conjugated anti-mouse and Alexa568-conjugated anti-rabbit antibodies after extensive washing with a wash buffer (10-mM Tris-HCl, [pH 7.4], 150-mM NaCl, and 0.05% Tween20). We mounted the samples with ProLong Diamond Antifade Mountant reagent with DAPI (Thermo Fisher) and observed them under a confocal laser scanning microscope (LSM710, Carl Zeiss).

Flow cytometric analysis

We treated the synchronized cells with or without 25-μM MNU for 1 h, then cultured them until harvesting by trypsin-EDTA treatment. We permeabilized the cells with PBS containing 0.1% Triton X-100 with 20-μg/mL propidium iodide and 40-μg/mL RNaseA and analyzed them using FACS Lyric (BD Biosciences) until the gated events reached 10,000.

Statistics

All experiments were repeated at least twice. Significant differences between two groups were calculated using student's *t*-test and those between >3 were determined using a one-way ANOVA with Kruskal–Wallis test. $p < 0.05$ is significant.

Results

FANCD2-knockout cells exhibit MMR-dependent MNU hypersensitivity

To determine the relevance of FANCD2 in the alkylating agent-induced mismatch repair-dependent DNA damage, we constructed two independent FANCD2-knockout (KO) cell lines using CRISPR/Cas9, then examined how the FANCD2-defect affected MNU sensitivity through a survival assay. The FANCD2-KO clones carry insertions or deletions in exon 3 of the FANCD2 gene alleles on chromosome 3, causing frameshift mutations and thereby producing a stop codon (Figure 1, Figure S1). Gene inactivation of FANCD2 gene was also confirmed by immunoblotting with a FANCD2-specific antibody and detected no band corresponding to FANCD2 in FANCD2-KO cells, which could be visibly observed in wild-type cells (Figure 1a). FANCD2 knockout did not affect the major MMR protein MSH2 and MLH1 expression levels.

We treated the FANCD2-KO cells with various MNU doses and counted the surviving colony numbers. Both FANCD2-KO cell lines exhibited high MNU sensitivity, whereas wild-type cells were little sensitive at such low concentrations (Figure 1b). Interestingly, two independent

siRNA-mediated MSH2 or MLH1 knockdown completely abolished this MNU hypersensitivity in the FANCD2-KO cell lines (Figure 1c, and d), suggesting that FANCD2 might contribute to overcoming the problems caused by the MMR complex-bound O^6-meG/T mismatch-containing DNA.

FANCD2 is ubiquitinated in response to MNU

In a previous study, our immunoblotting analysis revealed a FANCD2 band shift upon MNU administration [20]. To determine whether this was due to FANCD2 ubiquitination, we treated HA-tagged ubiquitin-expressing HeLa MR cells with MNU and prepared chromatin-bound fractions. We performed an immunoprecipitation assay using an anti-FANCD2 antibody and subjected the precipitated materials to immunoblotting with an anti-HA antibody (Figure 2a). We could detect a marked HA signal in the MNU-treated HA-tagged ubiquitin-expressing cells, whereas no such signal was visible in the control, indicating FANCD2 ubiquitination upon the MNU treatment. Similar results were obtained using MMC-treated or untreated cells, suggesting that MNU treatment also induces monoubiquitination of FANCD2 (Figure 2b).

FANCD2 forms nuclear foci and colocalizes with the MMR complex upon DNA alkylation

To determine FANCD2 function in the cellular response to alkylating agent-induced DNA damage, we examined the FANCD2 protein localization after MNU treatment using immunofluorescence microscopy (Figure 3a). The analysis showed that FANCD2 foci increased in response to MNU treatment in an MLH1-dependent manner (Figure 3b and S2), and that certain number of MLH1 foci colocalized with FANCD2 after the MNU treatment (Figure 3d). The number of MLH1 foci gradually increased with a FANCD2-independent manner 24 and 48 h after the treatment (Figure 3c), indicating that FANCD2 is dispensable for the association of MMR complex to the damaged site. Therefore, FANCD2 is recruited to the MMR complex-bound damaged chromatin.

FANCD2 defect enhances apoptosis induction upon MNU treatment

To precisely investigate the cell death process in FANCD2-KO cells, we synchronized them in the early S phase by double thymidine block, which we released following MNU treatment. Subsequently, we analyzed a series of cellular responses, such as cell cycle progression, checkpoint activation timing, and apoptosis induction (Figure 4).

Our flow cytometry analysis revealed that wild-type cells progressed smoothly to the S phase and reached the G1 phase 12 h after their release. The progression of the next cell cycle round was slightly delayed at the S phase at 18 h and arrested at the G2/M phase at 24–36 h, followed by the restart of the progression into the G1 phase without apoptosis induction. In contrast, FANCD2-KO cells exhibited slower cell cycle progression, and about half of the cells were still in the G2/M phase at 12 h. The progression was severely delayed in the upcoming S phase at 24 h and arrested at the G2/M phase

at 36 h, followed by a gradual increase in the sub-G1 population, indicating apoptosis induction (Figure 4a and b).

To confirm apoptotic cell death induction in the FANCD2-KO cells, we analyzed Caspase-9 and PARP1 cleavage by immunoblotting. The bands corresponding to cleaved Caspase-9 and PARP1 were visible at 48 h after the MNU treatment and more distinct at 60–72 h, whereas such bands could be hardly seen in the HeLa MR cells (Figure 4c). These results were consistent with those of the flow cytometry analysis, demonstrating that the hypersensitivity of the FANCD2-KO cells resulted from apoptosis induction following G2/M arrest.

Moreover, we analyzed the DNA damage response in HeLa MR and FANCD2-KO cells (Figure 4d, and S3). CHK1, a check point kinase that responds to replication stress, was phosphorylated in FANCD2-KO cells 18 h after the MNU treatment. The phosphorylation level was maintained until 48 h in FANCD2-KO cells. In contrast, the phosphorylation of CHK2, another DSB-responding kinase, was barely detactable in HeLa MR cells, whereas the level of CHK2 phosphorylation increased from 18 h and reached a peak at 36 and 60 h in FANCD2-KO cells. ATR and ATM, the upstream master kinases that activate CHK1 and CHK2, respectively, also appeared to be phosphorylated in FANCD2-KO cells with the kinetics similar to CHK1 and CHK2 activation (Figure S3). These results suggest that in MNU-treated FANCD2-KO cells, replication stress might be generated during the S phase in the upcoming cell cycle round and is processed to produce DSB, potentially leading to apoptosis induction.

Enhanced 53BP1 nuclear foci formation in FANCD2-KO cells upon MNU treatment

To examine whether DSB occurs in FANCD2-KO cells, we quantified the number of 53BP1 nuclear foci as a marker of DSB in synchronized cells collected at different time points after MNU treatment (Figure 5). We observed spontaneous 53BP1 foci formation at 0 h and, after the MNU treatment, the number of foci slightly increased until 24 h when the cells started to arrest at the second round of the G2/M phase both in HeLa MR and FANCD2-KO cells. However, we observed a dramatic increase in 53BP1 focus formation at 48 h in FANCD2-KO but not HeLa MR cells. This increase was strongly suppressed in siMLH1- or siMSH2-tranfected FANCD2-KO cells which exhibit resistance to the treatment with low dose of MNU (Figure 1d and S4). These results suggest that DSB accumulation might be a potential cause of the apoptotic cell death observed in FANCD2-KO cells after the MNU treatment and that FANCD2 protects the cells from lethal DSBs generated in the MMR-dependent DNA damage response to alkylating agents.

MNU hypersensitivity-related inefficient CtIP chromatin loading in FANCD2-KO cells

FANCD2 functions as a scaffold for proteins involved in homologous recombination repair, such as CtIP and RAD51, to restart stalled replication forks [27,31,32]. To assess whether FANCD2 recruits

homologous recombination factors to the MNU treatment-damaged chromatin, we subjected chromatin fractions of synchronized cells to immunoblot analysis (Figure 6a). The ubiquitinated form of FANCD2 was loaded on the chromatin and the amount of FANCD2 increased at 18–24 h when the cell cycle progression was delayed and arrested in the G2 phase after the MNU treatment in HeLa MR cells. MMR proteins, such as MSH2 and MLH1, were loaded and remained on the chromatin throughout the cell cycle progression both in HeLa MR and FANCD2-KO cells. In contrast, γH2AX and multiple phosphorylated forms of RPA, which respond to replication stress and DSBs [33], were visible in FANCD2-KO but not in HeLa MR cells (Figure 6b), consistent with the observed 53BP1-focus formation (Figure 5). CtIP and RAD51 were recruited to the chromatin in HeLa MR cells at 18 h when the cells progressed through the S to the G2 phases. However, FANCD2-KO cells failed to efficiently recruit both CtIP and RAD51 to the chromatin. Our immunofluorescence analysis indicated that CtIP partially colocalized with the MMR complex (data not shown) and confirmed that CtIP- and RAD51-nuclear foci formation were reduced in FANCD2-KO cells at 24 and 48 h compared with those in HeLa MR cells (Figure 7a, 7b, and S5).

To investigate the relevance of CtIP chromatin loading in MNU sensitivity, we subjected gene-specific siRNA-transfected CtIP-knockdown cells to a survival assay (Figure 7c). CtIP-knockdown cells became more sensitive to MNU than the control, suggesting that FANCD2 responds to MMR-dependent replication stress upon MNU exposure and might prevent the collapse of the replication fork by recruiting HR proteins, such as CtIP and RAD51.

Discussion

During the alkylating agent-triggered MMR-dependent apoptosis induction, futile repair cycles have been considered as the causes of ssDNA and DSB formation, leading to cell cycle arrest and apoptosis [15]. However, the detailed underlying molecular mechanisms explaining how cell cycle delay occurs in the second round of the S phase and how the DNA repair pathway contributes to counteracting apoptosis induction remain poorly understood. From this aspect, the FANCD2 band shift on the immunoblotting and FANCD2 foci formation in the nuclei after alkylating agents administration suggested FANCD2 involvement in the response to alkylated DNA damage [20]. In this study, we described that FANCD2 is ubiquitinated and colocalizes with the MMR complex upon MNU treatment, suggesting the recruitment of FANCD2 to the damaged chromatin, which suffers from MMR-dependent replication stress, which seems to be enhanced during cell cycle progression as ATR/CHK1 activation and S phase delay are more evident in the second round of the cell cycle (Figure 4 and S3) [15]. The enhanced replication stress in the second round of the S phase might be caused by the collision of the ongoing replication fork and preexisting MMR proteins on the damaged chromatin during the futile repair cycle.

The functional relationship between MMR and FANCD2 in the repair of replication stress caused by

MMC-induced ICL has been previously reported [34,35]. In response to ICLs, FANCD2 is monoubiquitinated, forming nuclear foci in an MSH2-dependent manner, but not MLH1-dependent manner. The hypersensitivity of FANCD2-deficient cells to MMC was unaltered by *MSH2* or *MLH1* knockdown. Our results indicating the requirement of MLH1 for FANCD2 foci formation (Figure S2) and the hypersensitivity of FANCD2-KO cells (Figure 1d) suggest that FANCD2 interacts with the MMR complex and is involved in O^6-meG-induced damage response through a different pathway than for ICL-induced damage response.

FANCD2 reportedly localizes to the site of stalled replication forks to protect them from excessive nucleolytic degradation of the nascent strand and to facilitate their restart by recruiting DNA repair proteins [22,27,36-38]. In addition, FANCD2 reportedly recruits CtIP and other HR proteins at stalled replication forks [32,39]. CtIP stabilizes the HU-induced stalled fork by preventing nascent DNA degradation by DNA2 [40]. FANCD2-dependent APH-mediated CtIP recruitment at the stalled replication fork stabilizes the forks. Furthermore, FANCD2 protects the forks CtIP-independently from MRE11-mediated degradation. MRE11 inhibition reportedly suppresses the FANCD2 depletion-triggered stalled fork degradation [27]. Consistent with the roles of FANCD2, we observed that FANCD2 depletion exacerbated cellular sensitivity to the alkylating agent MNU. Notably, MNU sensitivity was completely abolished upon siRNA-mediated MSH2 or MLH1 knockdown in FANCD2 KO cells. We also observed inefficient CtIP and RAD51 accumulation on the damaged chromatin in FANCD2-KO cells. Under such conditions, S phase progression was severely delayed and DSBs accumulated. Therefore, FANCD2 could be potentially required to protect stalled replication forks by recruiting CtIP and RAD51 on the damaged chromatin in MNU-treated cells. FANCD2-deficient cells might suffer from the excessive nascent strand degradation of the stalled forks followed by fork destabilization-related DSB formation. FANCD2-dependent CtIP and Rad51 chromatin loading could occur not only during replication fork perturbation but also after DSB formation following replication collapse [38].

Distinguishing whether CtIP would be recruited by FANCD2 at stalled replication forks or the DSB ends in response to MNU is currently impossible, as MMR-dependent replication fork arrest and replication collapse occur in close succession.

The FA pathway might be pivotal in coordinating the activities of several nucleases at the arrested replication fork. Among these enzymes, FAN1 interacts with the ubiquitinated K561 of FANCD2 via a UBZ domain [41-43]. We demonstrated that FAN1 coprecipitates with the MNU-provoked MMR complex and contributes to apoptosis induction, as FAN1 knockdown triggers MNU resistance [20].

Although FAN1-single knockdown did not particularly affect survival against MNU and FAN1 focus formation with MLH1 was partial, FAN1/EXO1/FEN1 triple knockdown cells were more resistant to the lethal MNU effect (unpublished data). Therefore, FANCD2 could potentially regulate the reactions catalyzed by multiple nucleases and contributes to stabilizing the arrested replication

fork.

MMR proteins were detected in FLAG pulled-down materials in FLAG-tagged FANCD2-expressing 293 T cells after HU treatment, suggesting a relationship between MMR and FANCD2 in replication fork repair [22]. Further proofs of this relationship have been recently reported, demonstrating that PolE P286R mutation-introduced abundant mismatches caused the accumulation of the MMR complex on the chromatin, preventing FANCD2 binding to the arrested replication fork, thereby leading to MRE11-mediated fork structure degradation and DSB formation [26]. Furthermore, MLH1 recruits FAN1 to expand the ssDNA region around mismatches, which could be converted to DSBs [20]. Therefore, MMR proteins might actively address the problem occurring at the replication fork toward apoptosis induction. In contrast, our data suggest that Fanconi-related proteins resolve the MMR-dependent replication stress due to the O^6-meG produced upon the alkylating agent treatment by recruiting HR-related proteins. Yeast genetics results demonstrated the requirement of Rad52 for the growth of yeast following alkylating agent treatments, suggesting HR pathway dependency to survive the cytotoxic effect of O^6-mG [15,44].

Therefore, how cells organize the balance between two opposing responses i.e., MMR function-related apoptosis induction and DNA repair system-assisted survival requires further investigation.

Alkylating anticancer drugs, such as temozolomide, are used to treat gliomas, although they exhibit low response rates and poor prognosis. Our results suggest that inhibiting FANCD2 function using specific FANCD2 inhibitors could potentially increase such drug efficacy.

Acknowledgments

The authors thank Dr Yoshimichi Nakatsu for helpful discussion.

Funding

This work was supported by the Promotion and Mutual Aid Corporation for Private Schools of Japan, The Science Research Promotion Fund, and JSPS KAKENHI Grant-in-Aid for Scientific research (C) Grant Number 22K09956 (to R.F.) and Grant Number 20K09915 (to M.H.).

Author Contribution

Conceptualization: Ryosuke Fujikane, Masumi Hidaka; Formal analysis investigation and resources: Sho Morita, Ryosuke Fujikane, Yuka Uechi; Writing - original draft preparation: Ryoske Fujikane; Writing - review and editing: Masumi Hidaka, Ryosuke Fujikane; Funding acquisition: Masumi Hidaka, Ryosuke Fujikane; Supervision: Masumi Hidaka, Takashi Matsuura.

Corresponding Author

Correspondence to Ryosuke Fujikane

Ethics Approval

Not applicable

Competing Interests

The authors declare no competing interests.

Figure Legends

Figure 1. FANCD2-KO cells display mismatch repair-dependent hypersensitivity to alkylating agents. (a) Expression of FANCD2 and the mismatch repair proteins MSH2 and MLH1 in HeLa MR and FANCD2-KO cells. Immunoblot analysis of whole-cell extracts from HeLa MR and FANCD2-KO cells using antibodies indicated. β-actin was used as a loading control. (b) Surviving fractions of HeLa MR and FANCD2-KO cells. The cells were treated with various MNU concentrations for 1 h and the surviving colonies were counted 10 days after the treatment. The values represent the mean of three independent experiments ± S.E. Student's *t*-test was used for statistical analysis. (c) MMR gene product expressions in siRNA-treated cells. Immunoblot analysis of whole-cell extracts using MSH2 and MLH1 antibodies. β-actin was used as a loading control. Representative images from two experiments are shown. Relative intensity of the bands from the image are indicated below. The asterisk represents nonspecific band (d) Surviving fraction of siRNA-treated cells after the MNU treatment. The experiments were performed as indicated in (b). ****: $p < 0.0001$, ***: $p < 0.001$, **: $p < 0.01$

Figure 2. FANCD2 is ubiquitinated upon MNU treatment. HeLa MR cells with or without HA-tagged ubiquitin expression were treated with 25-μM MNU (a) or 10-μM MMC (b) for 1 h. Chromatin fractions prepared from cells were subjected to immunoprecipitation using an anti-FANCD2 antibody. Chromatin-bound fractions (input) and precipitates (IP:FANCD2) were analyzed by immunoblotting using HA and FANCD2 antibodies.

Figure 3. FANCD2 forms nuclear foci upon MNU treatment. The cells were treated with or without 25-μM MNU for 1 h and permeabilized with 0.1% Triton X-100, followed by fixation with 4% paraformaldehyde. After blocking, immunofluorescence analysis was performed using FANCD2 and MLH1. The samples were mounted with Prolong Diamond antifade reagent with DAPI. Representative pictures from two experiments are shown. (b) The number of nuclear FANCD2 foci were counted and plotted as boxplot. Horizontal bars in boxes indicate the median, and P-values were derived from one-way ANOVA with Kruskal–Wallis test. Data was obtained from at least 182 nuclei

in several pictures from two experiments. (c) The number of nuclear MLH1 foci were counted and plotted as indicated in (b). (d) Percentages of nuclear MLH1 foci colocalized with FANCD2 in total MLH1 foci were plotted as indicated in (b). ****: $p < 0.0001$, **: $p < 0.01$, ns: not significant

Figure 4. FANCD2-KO cells display enhanced cellular response to MNU. (a) Synchronized cells in the early S phase (time 0 h), followed by 25-μM MNU treatment for 1 h as well as their release were analyzed by flow cytometry. The profiles were obtained from the cell numbers plotted according to the propidium iodide signal intensity. Representative plots from three experiments are shown. (b) Cell cycle profiles at the indicated time points in a stacked bar chart. The mean values from three experiments with S.E. are shown. Significant differences in G2/M phase and Sub-G1 phase between cell lines at the same time points calculated with student's *t*-test. **: $p < 0.01$, * $p < 0.05$. (c) Apoptotic events represented by Caspase-9 and PARP-1 cleavage were analyzed by immunoblotting using specific antibodies. The cells were treated with 25-μM MNU and the whole-cell extracts at the indicated time points after the treatment were collected and analyzed. β-actin was used as a loading control. (d) CHK1 and CHK2 kinases respond to MNU were analyzed by immunoblotting. Whole-cell extracts from cells treated with 25-μM MNU for 1 h were analyzed at the indicated time points using antibodies shown on the right. β-actin was used as a loading control. Representative images from three experiments are shown. Relative phosphorylation rates of the checkpoint proteins, derived from the values of quantified image are indicated below.

Figure 5. Double-strand breaks accumulate in FANCD2-KO cells after MNU treatment. The synchronized cells were treated or untreated with 25-μM MNU for 1 h and collected at the indicated times, followed by 0.1% Triton X-100 permeabilization, paraformaldehyde fixation, and anti-53BP1 antibody staining. (a) Representative images of 53BP1 foci upon MNU treatment. Representative pictures from two experiments are shown. (b) The number of nuclear 53BP1 foci were counted and plotted in boxplot. Bars are the mean value, and P-values were derived from one-way ANOVA with Kruskal–Wallis test. Data were obtained from several pictures from two experiments.

Figure 6. Aberration of CtIP and RAD51 chromatin loading in FANCD2-KO cells upon MNU treatment. (a) and (b) Chromatin fractions from 25-μM MNU-treated or -untreated synchronized cells were subjected to immunoblotting using antibodies indicated on the right of the panel. LAMIN A/C was used as a loading control. Representative blots from three experiments are shown. Relative intensities of bands are indicated below.

Figure 7. Attenuation of CtIP focus formation in FANCD2-KO cells after MNU treatment. (a) Cells treated with or without 25-μM MNU were collected at 24 or 48 h after the treatment, permeabilized,

and fixed, followed by immunostaining with an anti-CtIP antibody. (b) The number of CtIP foci in nuclei were counted and plotted as boxplot. Horizontal bars indicate the median, and P-values were derived from a one-way ANOVA with Kruskal–Wallis test. Data was obtained from ≥150 nuclei in several images from two experiments. (c) Surviving fraction upon CtIP siRNA knockdown. The siRNA-transfected cells were treated with various MNU concentrations and the surviving colonies were counted 10 days after the treatment. The data represent the mean values of at least three independent experiments ± S.E. CtIP expression levels in siRNA-transfected cells analyzed by immunoblotting using anti-CtIP antibody. β-actin was used as loading control. Relative intensities of bands from three experiments are shown.

Figure S1. CRISPR/Cas9 introduces insertions and deletions in exon 3 of the FANCD2 alleles. The nucleotide sequences of exon 3 of the wild-type allele and three alleles from each knockout clone are presented. The target locus was PCR-amplified, cloned into a T-vector, and sequenced. The under bar indicates the CRISPR/Cas9 target sequence. Premature stop codons are highlighted in bold lowercase letters. Dotted lines (---) and (ins) indicate the deletion and insertion sites, respectively.

Figure S2. FANCD2 foci formation upon MNU treatment is abrogated in MLH1-deficient cells. MLH1-deficient cells were treated with or without 25-μM MNU for 1 h and permeabilized with 0.1% Triton X-100, followed by fixation with 4% paraformaldehyde. After blocking, immunofluorescence analysis was performed using FANCD2 and MLH1 antibodies. The samples were mounted with Prolong Diamond antifade reagent with DAPI.

Figure S3. Activation of ATR and ATM after MNU treatment. Whole-cell extracts from cells treated with 25-μM MNU for 1 h were analyzed at the indicated time points using antibodies shown on the right. β-actin was used as a loading control. Relative phosphorylation rates of the checkpoint proteins, derived from the values of quantified image are indicated below.

Figure S4. Suppression of MNU-induced focus formation of 53BP1 in FANCD2-KO cells by knockdown of MMR genes. FANCD2-KO cells transfected with siRNA specific for MLH1 or MSH2 were treated with or without 25-μM MNU for 1 h and permeabilized with 0.1% Triton X-100, followed by fixation with 4% paraformaldehyde. After blocking, immunofluorescence analysis was performed using anti-53BP1 antibody. The number of nuclear foci were counted and plotted. Data was obtained from ≥93 nuclei in several images. Significant differences were calculated using one-way ANOVA with Kruskal–Wallis test. ****: $p < 0.0001$, **: $p < 0.01$.

Figure S5. Attenuation of RAD51 focus formation in FANCD2-KO cells after MNU treatment. Cells

treated with or without 25-μM MNU were collected at 24 or 48 h after treatment, permeabilized, and fixed, followed by immunostaining with an anti-RAD51 antibody. The number of RAD51 foci in the nuclei were counted and plotted. Data was obtained from ≥91 nuclei in several images. P-values were derived from a one-way ANOVA with Kruskal–Wallis test. ****: $p < 0.0001$.

References

1. Desai A, Gerson S (2014) Exo1 independent DNA mismatch repair involves multiple compensatory nucleases. DNA Repair (Amst) 21: 55-64. 10.1016/j.dnarep.2014.06.005I.
2. Constantin N, Dzantiev L, Kadyrov FA, Modrich P (2005) Human mismatch repair: reconstitution of a nick-directed bidirectional reaction. The Journal of biological chemistry 280: 39752-39761. 10.1074/jbc.M509701200I.
3. Fang W, Modrich P (1993) Human strand-specific mismatch repair occurs by a bidirectional mechanism similar to that of the bacterial reaction. The Journal of biological chemistry 268: 11838-11844.
4. Karran P (2001) Mechanisms of tolerance to DNA damaging therapeutic drugs. Carcinogenesis 22: 1931-1937.
5. Karran P, Macpherson P, Ceccotti S, Dogliotti E, Griffin S, Bignami M (1993) O6-methylguanine residues elicit DNA repair synthesis by human cell extracts. The Journal of biological chemistry 268: 15878-15886.
6. Kaina B, Ziouta A, Ochs K, Coquerelle T (1997) Chromosomal instability, reproductive cell death and apoptosis induced by O6-methylguanine in Mex-, Mex+ and methylation-tolerant mismatch repair compromised cells: facts and models. Mutation research 381: 227-241. 10.1016/s0027-5107(97)00187-5I.
7. Tominaga Y, Tsuzuki T, Shiraishi A, Kawate H, Sekiguchi M (1997) Alkylation-induced apoptosis of embryonic stem cells in which the gene for DNA-repair, methyltransferase, had been disrupted by gene targeting. Carcinogenesis 18: 889-896.
8. Kaina B, Christmann M, Naumann S, Roos WP (2007) MGMT: key node in the battle against genotoxicity, carcinogenicity and apoptosis induced by alkylating agents. DNA Repair (Amst) 6: 1079-1099. 10.1016/j.dnarep.2007.03.008I.
9. Hidaka M, Takagi Y, Takano TY, Sekiguchi M (2005) PCNA-MutSalpha-mediated binding of MutLalpha to replicative DNA with mismatched bases to induce apoptosis in human cells. Nucleic Acids Res 33: 5703-5712. 10.1093/nar/gki878I.
10. Stojic L, Mojas N, Cejka P, Di Pietro M, Ferrari S, Marra G, Jiricny J (2004) Mismatch repair-dependent G2 checkpoint induced by low doses of SN1 type methylating agents requires the ATR kinase. Genes & development 18: 1331-1344. 10.1101/gad.294404I.
11. Ganesa S, Sule A, Sundaram RK, Bindra RS (2022) Mismatch repair proteins play a role in ATR activation upon temozolomide treatment in MGMT-methylated glioblastoma. Scientific reports

12: 5827. 10.1038/s41598-022-09614-xI.

12. Hickman M, Samson L (2004) Apoptotic signaling in response to a single type of DNA lesion, O(6)-methylguanine. Mol Cell 14: 105-116.
13. Fujikane R, Sanada M, Sekiguchi M, Hidaka M (2012) The identification of a novel gene, MAPO2, that is involved in the induction of apoptosis triggered by O(6)-methylguanine. PloS one 7: e44817. 10.1371/journal.pone.0044817I.
14. Fujikane R, Komori K, Sekiguchi M, Hidaka M (2016) Function of high-mobility group A proteins in the DNA damage signaling for the induction of apoptosis. Scientific reports 6: 31714. 10.1038/srep31714I.
15. Mojas N, Lopes M, Jiricny J (2007) Mismatch repair-dependent processing of methylation damage gives rise to persistent single-stranded gaps in newly replicated DNA. Genes & development 21: 3342-3355. 10.1101/gad.455407I.
16. Olivera Harris M, Kallenberger L, Artola Boran M, Enoiu M, Costanzo V, Jiricny J (2015) Mismatch repair-dependent metabolism of O6-methylguanine-containing DNA in Xenopus laevis egg extracts. DNA Repair (Amst) 28: 1-7. 10.1016/j.dnarep.2015.01.014I.
17. Yoshioka K, Yoshioka Y, Hsieh P (2006) ATR kinase activation mediated by MutSalpha and MutLalpha in response to cytotoxic O6-methylguanine adducts. Mol Cell 22: 501-510. 10.1016/j.molcel.2006.04.023I.
18. Liu Y, Fang Y, Shao H, Lindsey-Boltz L, Sancar A, Modrich P (2010) Interactions of human mismatch repair proteins MutSalpha and MutLalpha with proteins of the ATR-Chk1 pathway. The Journal of biological chemistry 285: 5974-5982. 10.1074/jbc.M109.076109I.
19. Pabla N, Ma Z, McIlhatton MA, Fishel R, Dong Z (2011) hMSH2 recruits ATR to DNA damage sites for activation during DNA damage-induced apoptosis. The Journal of biological chemistry 286: 10411-10418. 10.1074/jbc.M110.210989I.
20. Rikitake M, Fujikane R, Obayashi Y, Oka K, Ozaki M, Hidaka M (2020) MLH1-mediated recruitment of FAN1 to chromatin for the induction of apoptosis triggered by O(6) -methylguanine. Genes to cells : devoted to molecular & cellular mechanisms 25: 175-186. 10.1111/gtc.12748I.
21. Chen CC, Taniguchi T, D'Andrea A (2007) The Fanconi anemia (FA) pathway confers glioma resistance to DNA alkylating agents. Journal of molecular medicine 85: 497-509. 10.1007/s00109-006-0153-2I.
22. Lossaint G, Larroque M, Ribeyre C, Bec N, Larroque C, Decaillet C, Gari K, Constantinou A (2013) FANCD2 binds MCM proteins and controls replisome function upon activation of s phase checkpoint signaling. Mol Cell 51: 678-690. 10.1016/j.molcel.2013.07.023I.
23. Lachaud C, Moreno A, Marchesi F, Toth R, Blow JJ, Rouse J (2016) Ubiquitinated Fancd2 recruits Fan1 to stalled replication forks to prevent genome instability. Science 351: 846-849. 10.1126/science.aad5634I.

24. Meetei AR, de Winter JP, Medhurst AL, Wallisch M, Waisfisz Q, van de Vrugt HJ, Oostra AB, Yan Z, Ling C, Bishop CE, Hoatlin ME, Joenje H, Wang W (2003) A novel ubiquitin ligase is deficient in Fanconi anemia. Nature genetics 35: 165-170. 10.1038/ng1241I.

25. Yamamoto K, Kobayashi S, Tsuda M, Kurumizaka H, Takata M, Kono K, Jiricny J, Takeda S, Hirota K (2011) Involvement of SLX4 in interstrand cross-link repair is regulated by the Fanconi anemia pathway. Proceedings of the National Academy of Sciences of the United States of America 108: 6492-6496.

26. Zhang J, Zhao X, Liu L, Li HD, Gu L, Castrillon DH, Li GM (2022) The mismatch recognition protein MutSalpha promotes nascent strand degradation at stalled replication forks. Proceedings of the National Academy of Sciences of the United States of America 119: e2201738119. 10.1073/pnas.2201738119I.

27. Schlacher K, Wu H, Jasin M (2012) A distinct replication fork protection pathway connects Fanconi anemia tumor suppressors to RAD51-BRCA1/2. Cancer cell 22: 106-116. 10.1016/j.ccr.2012.05.015I.

28. Takeishi Y, Fujikane R, Rikitake M, Obayashi Y, Sekiguchi M, Hidaka M (2020) SMARCAD1-mediated recruitment of the DNA mismatch repair protein MutLalpha to MutSalpha on damaged chromatin induces apoptosis in human cells. The Journal of biological chemistry 295: 1056-1065. 10.1074/jbc.RA119.008854I.

29. Concordet JP, Haeussler M (2018) CRISPOR: intuitive guide selection for CRISPR/Cas9 genome editing experiments and screens. Nucleic Acids Res 46: W242-W245. 10.1093/nar/gky354I.

30. Ran FA, Hsu PD, Wright J, Agarwala V, Scott DA, Zhang F (2013) Genome engineering using the CRISPR-Cas9 system. Nature protocols 8: 2281-2308. 10.1038/nprot.2013.143I.

31. Sato K, Shimomuki M, Katsuki Y, Takahashi D, Kobayashi W, Ishiai M, Miyoshi H, Takata M, Kurumizaka H (2016) FANCI-FANCD2 stabilizes the RAD51-DNA complex by binding RAD51 and protects the 5'-DNA end. Nucleic Acids Res 44: 10758-10771. 10.1093/nar/gkw876I.

32. Yeo JE, Lee EH, Hendrickson EA, Sobeck A (2014) CtIP mediates replication fork recovery in a FANCD2-regulated manner. Human molecular genetics 23: 3695-3705. 10.1093/hmg/ddu078I.

33. Ciccia A, Elledge SJ (2010) The DNA damage response: making it safe to play with knives. Mol Cell 40: 179-204. 10.1016/j.molcel.2010.09.019I.

34. Williams SA, Wilson JB, Clark AP, Mitson-Salazar A, Tomashevski A, Ananth S, Glazer PM, Semmes OJ, Bale AE, Jones NJ, Kupfer GM (2011) Functional and physical interaction between the mismatch repair and FA-BRCA pathways. Human molecular genetics 20: 4395-4410. 10.1093/hmg/ddr366I.

35. Huang M, Kennedy R, Ali AM, Moreau LA, Meetei AR, D'Andrea AD, Chen CC (2011) Human MutS and FANCM complexes function as redundant DNA damage sensors in the Fanconi Anemia pathway. DNA Repair (Amst) 10: 1203-1212. 10.1016/j.dnarep.2011.09.006I.

36. Tian Y, Shen X, Wang R, Klages-Mundt NL, Lynn EJ, Martin SK, Ye Y, Gao M, Chen J, Schlacher K, Li L (2017) Constitutive role of the Fanconi anemia D2 gene in the replication stress response. The Journal of biological chemistry 292: 20184-20195. 10.1074/jbc.M117.814780I.

37. Dungrawala H, Rose KL, Bhat KP, Mohni KN, Glick GG, Couch FB, Cortez D (2015) The Replication Checkpoint Prevents Two Types of Fork Collapse without Regulating Replisome Stability. Mol Cell 59: 998-1010. 10.1016/j.molcel.2015.07.030I.

38. Rickman K, Smogorzewska A (2019) Advances in understanding DNA processing and protection at stalled replication forks. The Journal of cell biology 218: 1096-1107. 10.1083/jcb.201809012I.

39. Unno J, Itaya A, Taoka M, Sato K, Tomida J, Sakai W, Sugasawa K, Ishiai M, Ikura T, Isobe T, Kurumizaka H, Takata M (2014) FANCD2 binds CtIP and regulates DNA-end resection during DNA interstrand crosslink repair. Cell reports 7: 1039-1047. 10.1016/j.celrep.2014.04.005I.

40. Przetocka S, Porro A, Bolck HA, Walker C, Lezaja A, Trenner A, von Aesch C, Himmels SF, D'Andrea AD, Ceccaldi R, Altmeyer M, Sartori AA (2018) CtIP-Mediated Fork Protection Synergizes with BRCA1 to Suppress Genomic Instability upon DNA Replication Stress. Mol Cell 72: 568-582 e566. 10.1016/j.molcel.2018.09.014I.

41. Yoshikiyo K, Kratz K, Hirota K, Nishihara K, Takata M, Kurumizaka H, Horimoto S, Takeda S, Jiricny J (2010) KIAA1018/FAN1 nuclease protects cells against genomic instability induced by interstrand cross-linking agents. Proceedings of the National Academy of Sciences of the United States of America 107: 21553-21557.

42. MacKay C, Declais AC, Lundin C, Agostinho A, Deans AJ, MacArtney TJ, Hofmann K, Gartner A, West SC, Helleday T, Lilley DM, Rouse J (2010) Identification of KIAA1018/FAN1, a DNA repair nuclease recruited to DNA damage by monoubiquitinated FANCD2. Cell 142: 65-76. 10.1016/j.cell.2010.06.021I.

43. Smogorzewska A, Desetty R, Saito TT, Schlabach M, Lach FP, Sowa ME, Clark AB, Kunkel TA, Harper JW, Colaiacovo MP, Elledge SJ (2010) A genetic screen identifies FAN1, a Fanconi anemia-associated nuclease necessary for DNA interstrand crosslink repair. Mol Cell 39: 36-47. 10.1016/j.molcel.2010.06.023I.

44. Cejka P, Mojas N, Gillet L, Schar P, Jiricny J (2005) Homologous recombination rescues mismatch-repair-dependent cytotoxicity of S(N)1-type methylating agents in S. cerevisiae. Current biology : CB 15: 1395-1400. 10.1016/j.cub.2005.07.032I.

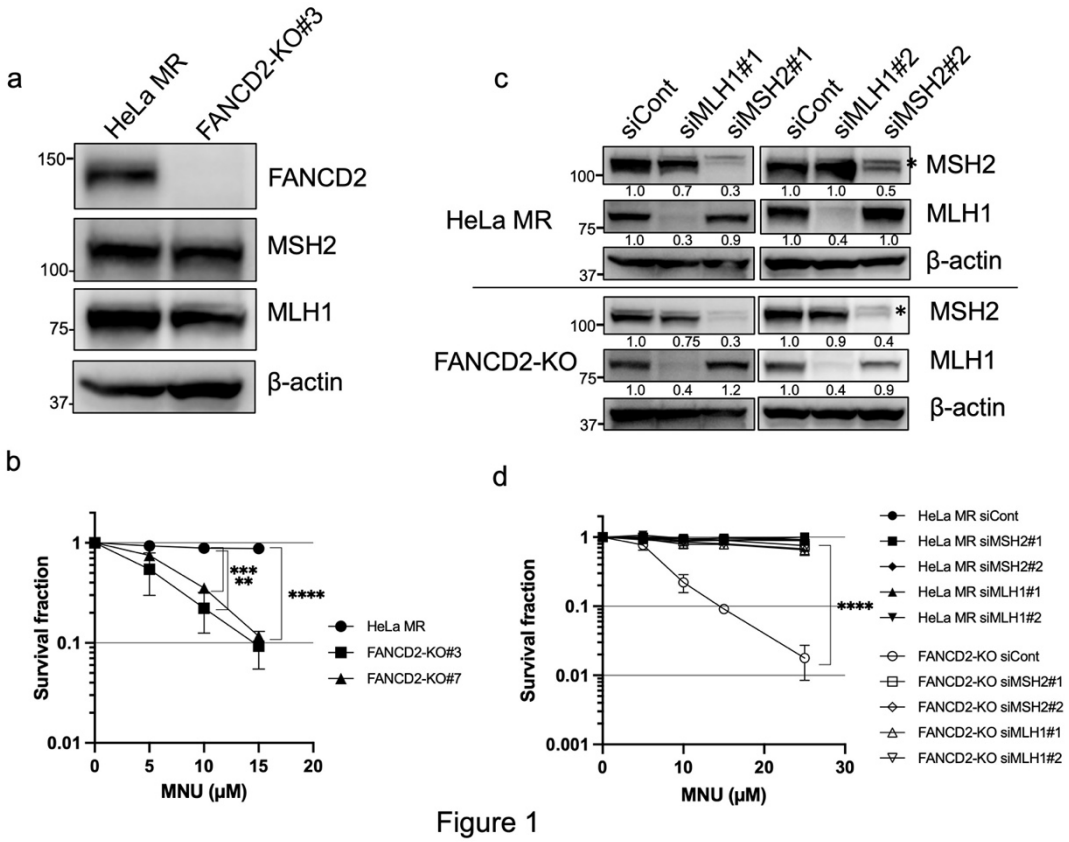

Figure 1

Figure 1. FANCD2-KO cells display mismatch repair-dependent hypersensitivity to alkylating agents. (a) Expression of FANCD2 and the mismatch repair proteins MSH2 and MLH1 in HeLa MR and FANCD2-KO cells. Immunoblot analysis of whole-cell extracts from HeLa MR and FANCD2-KO cells using antibodies indicated. β-actin was used as a loading control. (b) Surviving fractions of HeLa MR and FANCD2-KO cells. The cells were treated with various MNU concentrations for 1 h and the surviving colonies were counted 10 days after the treatment. The values represent the mean of three independent experiments ± S.E. Student's *t*-test was used for statistical analysis. (c) MMR gene product expressions in siRNA-treated cells. Immunoblot analysis of whole-cell extracts using MSH2 and MLH1 antibodies. β-actin was used as a loading control. Representative images from two experiments are shown. Relative intensity of the bands from the image are indicated below. The asterisk represents nonspecific band (d) Surviving fraction of siRNA-treated cells after the MNU treatment. The experiments were performed as indicated in (b). ****: $p < 0.0001$, ***: $p < 0.001$, **: $p < 0.01$

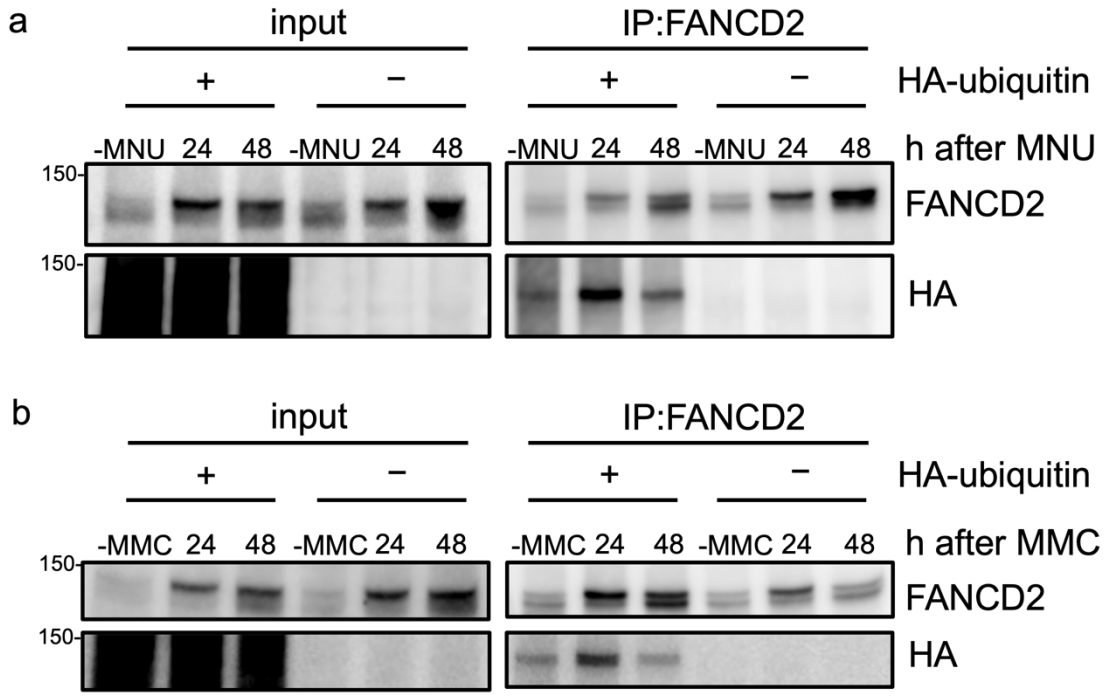

Figure 2

Figure 2. FANCD2 is ubiquitinated upon MNU treatment. HeLa MR cells with or without HA-tagged ubiquitin expression were treated with 25-μM MNU (a) or 10-μM MMC (b) for 1 h. Chromatin fractions prepared from cells were subjected to immunoprecipitation using an anti-FANCD2 antibody. Chromatin-bound fractions (input) and precipitates (IP:FANCD2) were analyzed by immunoblotting using HA and FANCD2 antibodies.

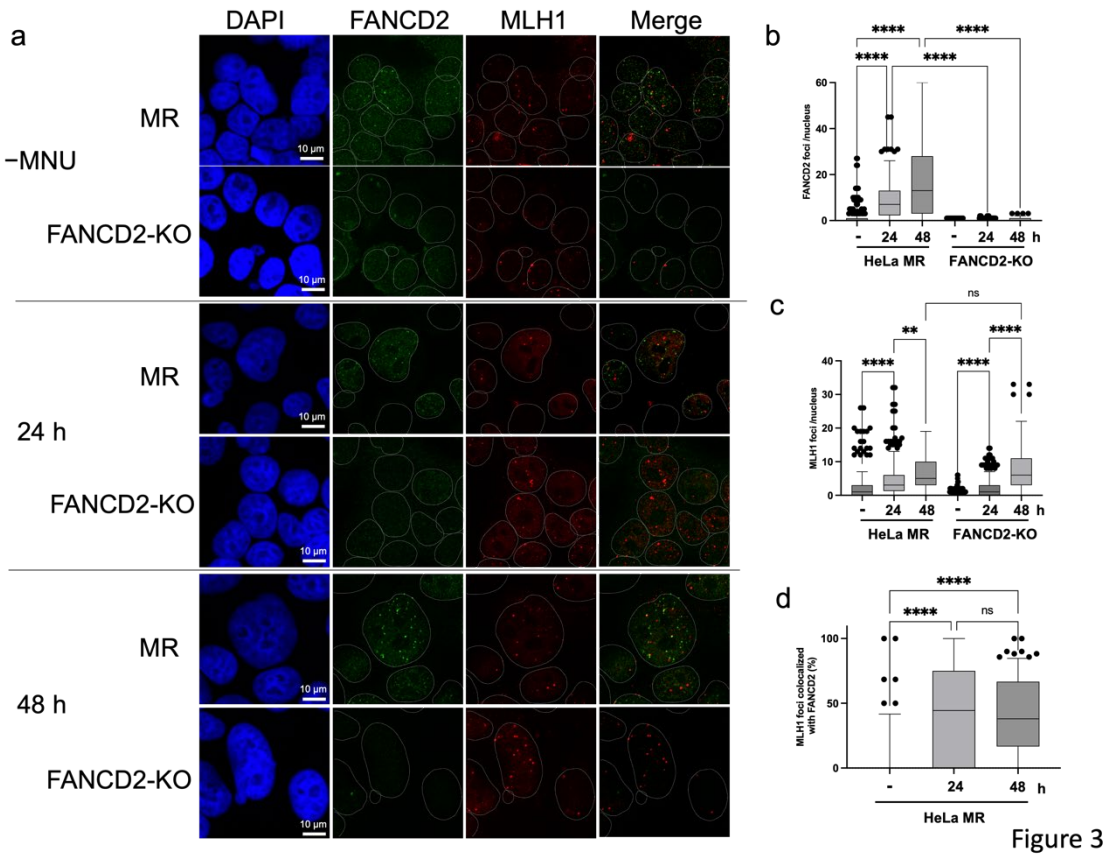

Figure 3. FANCD2 forms nuclear foci upon MNU treatment. The cells were treated with or without 25-µM MNU for 1 h and permeabilized with 0.1% Triton X-100, followed by fixation with 4% paraformaldehyde. After blocking, immunofluorescence analysis was performed using FANCD2 and MLH1. The samples were mounted with Prolong Diamond antifade reagent with DAPI. Representative pictures from two experiments are shown. (b) The number of nuclear FANCD2 foci were counted and plotted as boxplot. Horizontal bars in boxes indicate the median, and P-values were derived from one-way ANOVA with Kruskal–Wallis test. Data was obtained from at least 182 nuclei in several pictures from two experiments. (c) The number of nuclear MLH1 foci were counted and plotted as indicated in (b). (d) Percentages of nuclear MLH1 foci colocalized with FANCD2 in total MLH1 foci were plotted as indicated in (b). ****: $p < 0.0001$, **: $p < 0.01$, ns: not significant.

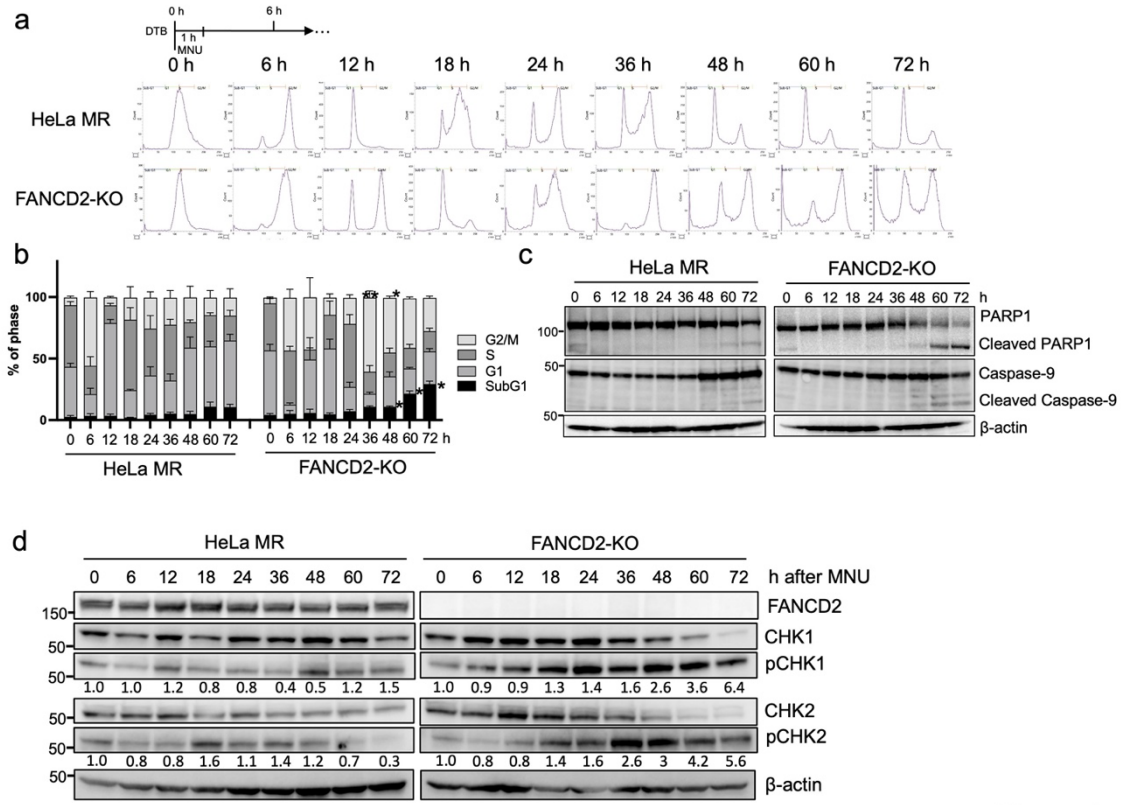

Figure 4

Figure 4. FANCD2-KO cells display enhanced cellular response to MNU. (a) Synchronized cells in the early S phase (time 0 h), followed by 25-μM MNU treatment for 1 h as well as their release were analyzed by flow cytometry. The profiles were obtained from the cell numbers plotted according to the propidium iodide signal intensity. Representative plots from three experiments are shown. (b) Cell cycle profiles at the indicated time points in a stacked bar chart. The mean values from three experiments with S.E. are shown. Significant differences in G2/M phase and Sub-G1 phase between cell lines at the same time points calculated with student's *t*-test. **: $p < 0.01$, * $p < 0.05$. (c) Apoptotic events represented by Caspase-9 and PARP-1 cleavage were analyzed by immunoblotting using specific antibodies. The cells were treated with 25-μM MNU and the whole-cell extracts at the indicated time points after the treatment were collected and analyzed. β-actin was used as a loading control. (d) CHK1 and CHK2 kinases respond to MNU were analyzed by immunoblotting. Whole-cell extracts from cells treated with 25-μM MNU for 1 h were analyzed at the indicated time points using antibodies shown on the right. β-actin was used as a loading control. Representative images from three experiments are shown. Relative phosphorylation rates of the checkpoint proteins, derived from the values of quantified image are indicated below.

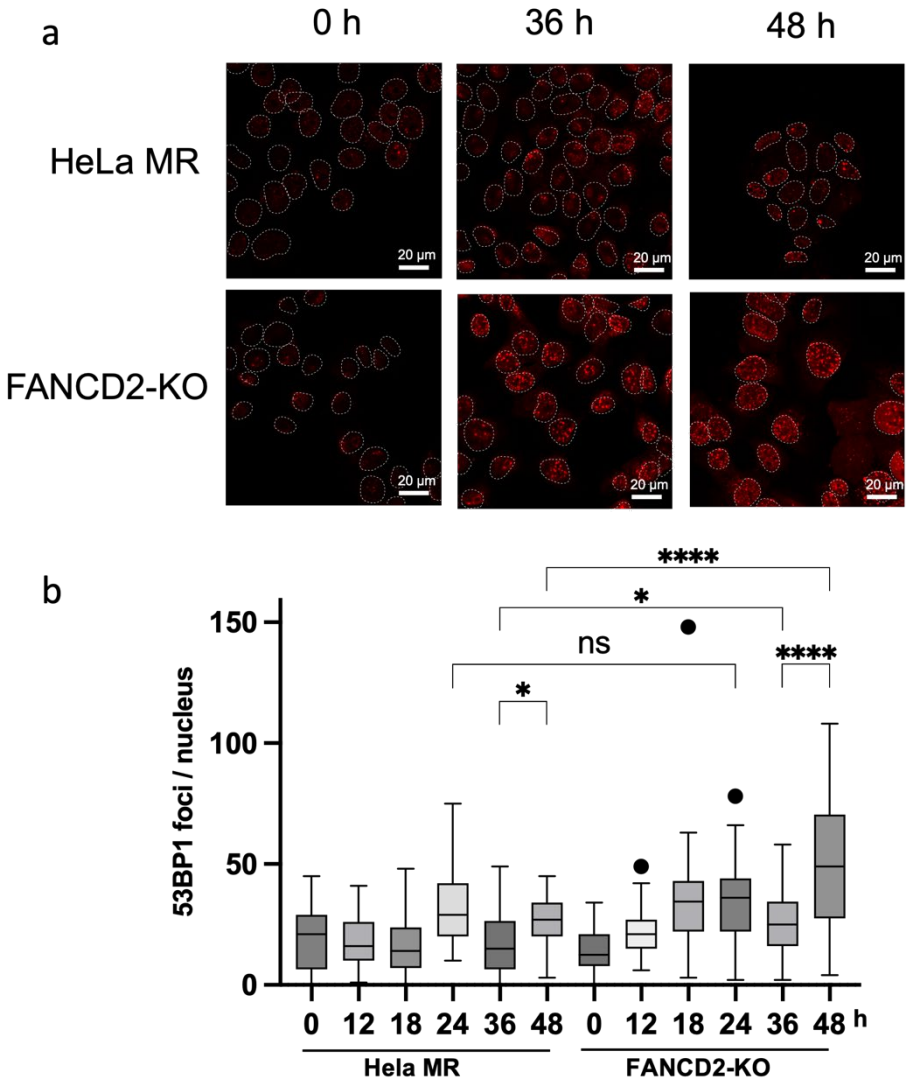

Figure 5

Figure 5. Double-strand breaks accumulate in FANCD2-KO cells after MNU treatment. The synchronized cells were treated or untreated with 25-µM MNU for 1 h and collected at the indicated times, followed by 0.1% Triton X-100 permeabilization, paraformaldehyde fixation, and anti-53BP1 antibody staining. (a) Representative images of 53BP1 foci upon MNU treatment. Representative pictures from two experiments are shown. (b) The number of nuclear 53BP1 foci were counted and plotted in boxplot. Bars are the mean value, and P-values were derived from one-way ANOVA with Kruskal–Wallis test. Data were obtained from several pictures from two experiments.

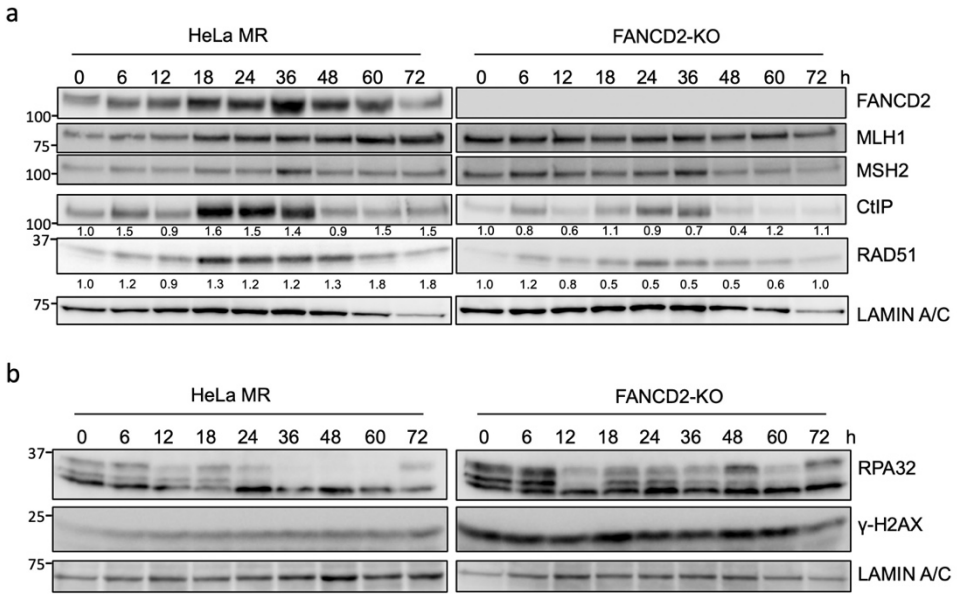

Figure 6

Figure 6. Aberration of CtIP and RAD51 chromatin loading in FANCD2-KO cells upon MNU treatment. (a) and (b) Chromatin fractions from 25-μM MNU-treated or -untreated synchronized cells were subjected to immunoblotting using antibodies indicated on the right of the panel. LAMIN A/C was used as a loading control. Representative blots from three experiments are shown. Relative intensities of bands are indicated below.

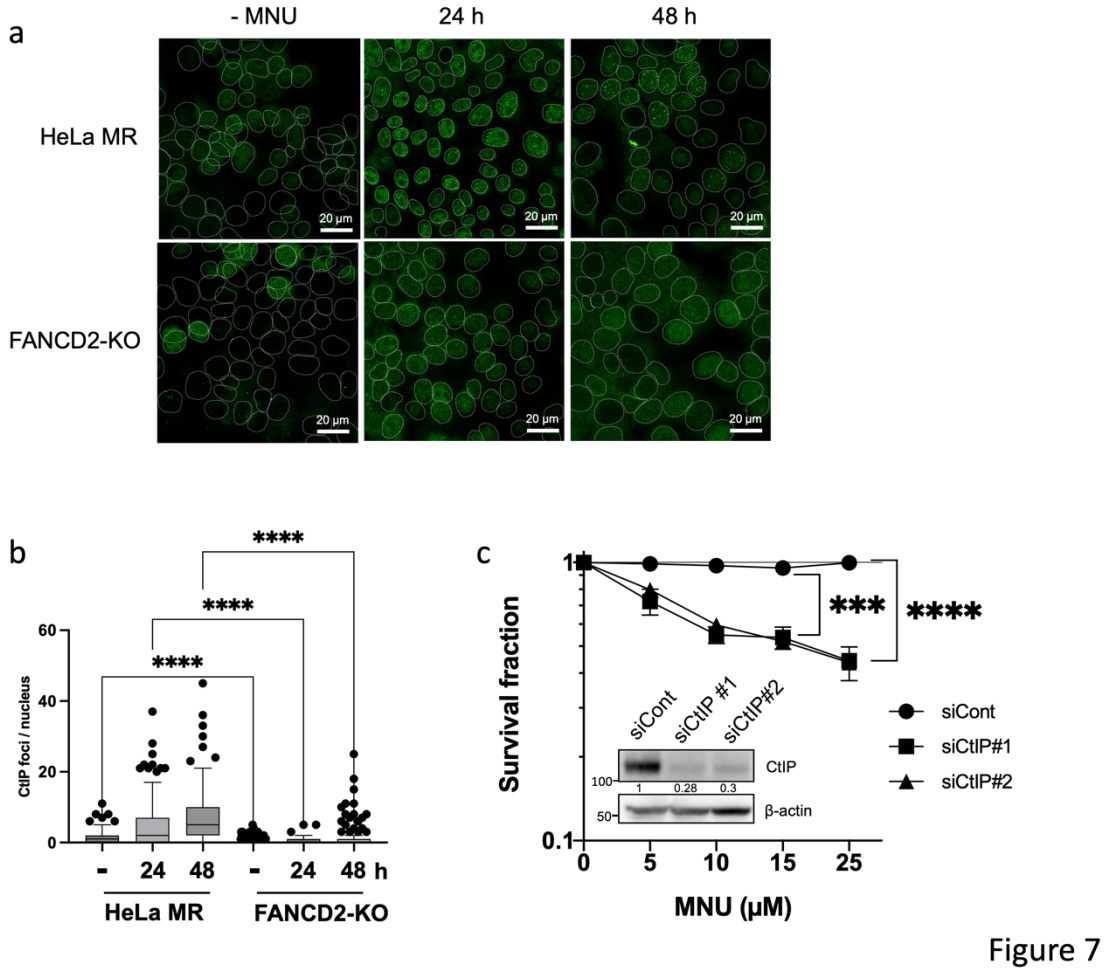

Figure 7

Figure 7. Attenuation of CtIP focus formation in FANCD2-KO cells after MNU treatment. (a) Cells treated with or without 25-μM MNU were collected at 24 or 48 h after the treatment, permeabilized, and fixed, followed by immunostaining with an anti-CtIP antibody. (b) The number of CtIP foci in nuclei were counted and plotted as boxplot. Horizontal bars indicate the median, and P-values were derived from a one-way ANOVA with Kruskal–Wallis test. Data was obtained from ≥150 nuclei in several images from two experiments. (c) Surviving fraction upon CtIP siRNA knockdown. The siRNA-transfected cells were treated with various MNU concentrations and the surviving colonies were counted 10 days after the treatment. The data represent the mean values of at least three independent experiments ± S.E. CtIP expression levels in siRNA-transfected cells analyzed by immunoblotting using anti-CtIP antibody. β-actin was used as loading control. Relative intensities of bands from three experiments are shown.

Figure S1. CRISPR/Cas9 introduces insertions and deletions in exon 3 of the FANCD2 alleles. The nucleotide sequences of exon 3 of the wild-type allele and three alleles from each knockout clone are presented. The target locus was PCR-amplified, cloned into a T-vector, and sequenced. The under bar indicates the CRISPR/Cas9 target sequence. Premature stop codons are highlighted in bold lowercase letters. Dotted lines (---) and (ins) indicate the deletion and insertion sites, respectively.

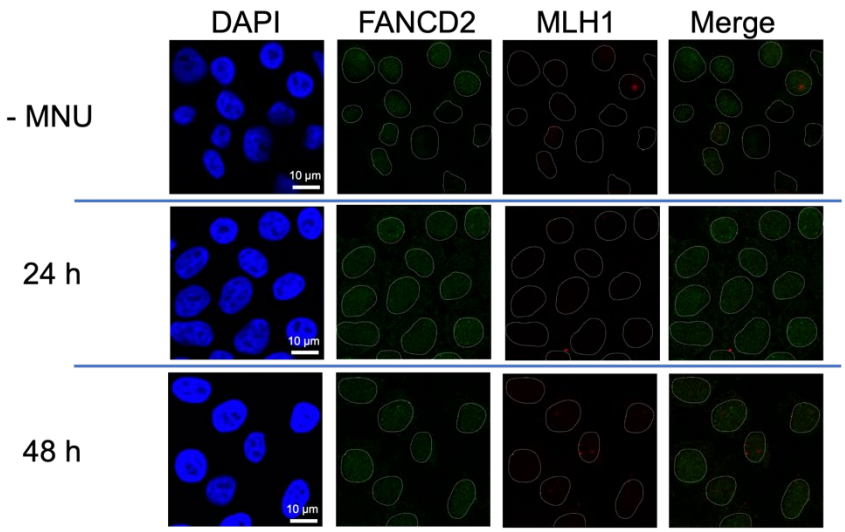

Figure S2

Figure S2. FANCD2 foci formation upon MNU treatment is abrogated in MLH1-deficient cells. MLH1-deficient cells were treated with or without 25-μM MNU for 1 h and permeabilized with 0.1% Triton X-100, followed by fixation with 4% paraformaldehyde. After blocking, immunofluorescence analysis was performed using FANCD2 and MLH1 antibodies. The samples were mounted with Prolong Diamond antifade reagent with DAPI.

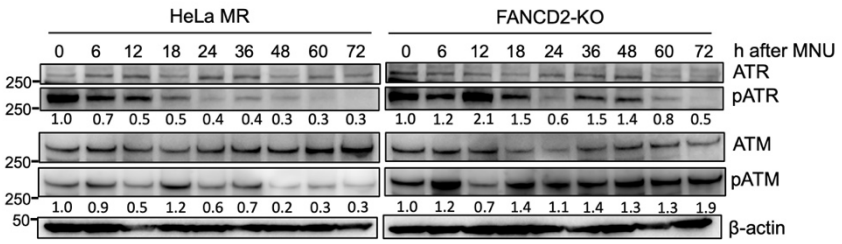

Figure S3

Figure S3. Activation of ATR and ATM after MNU treatment. Whole-cell extracts from cells treated with 25-μM MNU for 1 h were analyzed at the indicated time points using antibodies shown on the right. β-actin was used as a loading control. Relative phosphorylation rates of the checkpoint proteins, derived from the values of quantified image are indicated below.

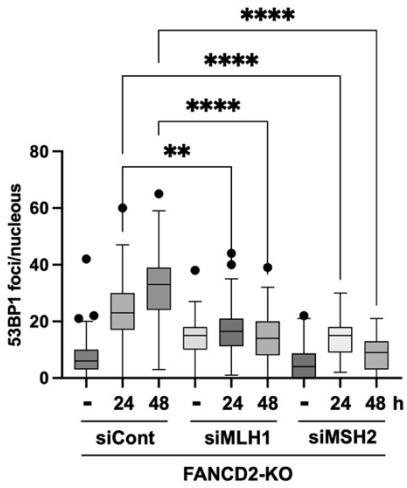

Figure S4

Figure S4. Suppression of MNU-induced focus formation of 53BP1 in FANCD2-KO cells by knockdown of MMR genes. FANCD2-KO cells transfected with siRNA specific for MLH1 or MSH2 were treated with or without 25-μM MNU for 1 h and permeabilized with 0.1% Triton X-100, followed by fixation with 4% paraformaldehyde. After blocking, immunofluorescence analysis was performed using anti-53BP1 antibody. The number of nuclear foci were counted and plotted. Data was obtained from ≥93 nuclei in several images. Significant differences were calculated using one-way ANOVA with Kruskal–Wallis test. ****: $p < 0.0001$, **: $p < 0.01$.

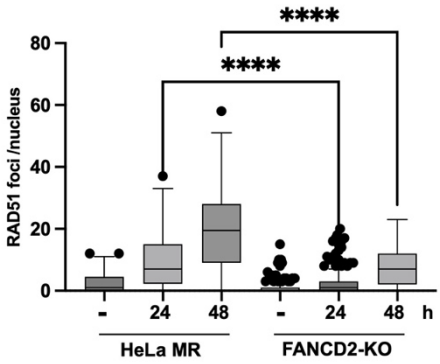

Figure S5

Figure S5. Attenuation of RAD51 focus formation in FANCD2-KO cells after MNU treatment. Cells treated with or without 25-μM MNU were collected at 24 or 48 h after treatment, permeabilized, and fixed, followed by immunostaining with an anti-RAD51 antibody. The number of RAD51 foci in the nuclei were counted and plotted. Data was obtained from ≥91 nuclei in several images. P-values were derived from a one-way ANOVA with Kruskal–Wallis test. ****: $p < 0.0001$.